Title
Mechanical Modeling and Optimal Model-based Design of a Soft Pneumatic Actuator

ISBN
9798350332223

Authors
Yang, Wu-Te
Stuart, Hannah S
Tomizuka, Masayoshi

Publication Date
2023-04-07

DOI
10.1109/robosoft55895.2023.10122083

Mechanical Modeling and Optimal Model-based Design of a Soft Pneumatic Actuator

Wu-Te Yang[1], Hannah S. Stuart[2], and Masayoshi Tomizuka[1]

***Abstract*— Soft pneumatic actuators are widely used for soft grippers, which are known for their compliance as compared with traditional grippers. The generated force/torque of soft pneumatic actuators directly determines the grasping force. This paper introduces a computationally efficient soft pneumatic actuator (SPA) design methodology. The complex structure of the pneumatic actuator is approximated by a cantilever beam. The relationship between input pressure and output torque is derived by standard mechanical analysis. The design problem is formulated as a model-based optimization problem by treating the input-output mathematical model as the objective function. By solving the optimization problem, the optimal design parameters are obtained. Finite element analysis is applied to preliminarily verify the design parameters without the time-consuming fabrication of many actuators. Three soft actuators with different design parameter sets were fabricated to validate the optimal parameters. This work shows the utility of surprisingly simple calculations and assumptions for rapid parametric design studies.**

I. INTRODUCTION

The soft robotics is gaining increasing popularity. Unlike conventional robots, soft robots possess inherent compliance. This advantage gives soft robots the potential to adapt to unknown environments [1], [2], ensures the safety of human-robot collaboration [3], and enables them to deal with fragile objects in the food and agriculture industry [4]. The performance of soft robots depends on the gripping force of soft actuators. Several types of soft actuators include electroactive polymers, cable-driven, shape memory alloy, and pneumatic actuators [5]. Pneumatic actuators are favorable for building soft robotic systems [5], [6] because they are lightweight and low-cost, and provide high power density. However, their complex geometric shapes and mechanics present computational challenges in optimal design.

Recent works [7]–[13] applied finite element analysis (FEA) with optimization methods to explore dimensional parameters of SPAs. Another common approach is to mimic structures found in nature [14], [15], such as the octopus arm-inspired tapered actuator [16], [17], to bypass formal optimization. Although these design approaches produce functional outcomes, there remain issues in producing efficient mathematical modeling and effort-saving optimization formulation for SPA design [9]. For example, optimal design parameters are often obtained through trial-and-error, numerous simulations, or tedious experiments [9]. These processes leads to a long development time of new pneumatic actuators for different use cases.

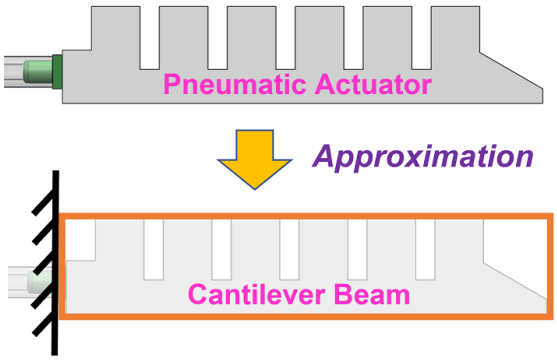

Fig. 1. The complex structure of the soft pneumatic actuator has been approximated as a cantilever beam for rapid optimization through mechanical analysis.

This paper proposes an efficient model-based optimal design method for SPAs. Firstly, we treat the complex-shaped structure of the pneumatic actuator as a cantilever beam, as depicted in Fig. 1. The approximated structure is analyzed by standard mechanical methods to get the relationship between input air pressure and output torque [18]. Then, the design problem is transformed into an optimization problem, and the derived mathematical model serves as the objective function. The optimal design parameters are searched and obtained by solving the optimization problem. Preliminary tests are conducted by the FEA simulation. Pneumatic actuators are then fabricated to validate the modelling method with experiments. These pneumatic actuators achieve more output torque and bending angles than ones reported in another recent work [3].

Several pneumatic actuator design approaches have been proposed recently. Demir et al. [3] utilized a machine learning algorithm to model the performance of pneumatic actuators with FEA simulation data. The model was used to search for the optimal design parameters under different constraints. In our work, we analyze and find the mathematical relationship between input and output to search for the optimal parameters. Polygerinos et al. [19] attempted to relate the pressure change and the output torque of a soft pneumatic glove; however, the analysis relies on complex mechanical models, and several material properties need to

[1]The authors are with Department of Mechanical Engineering, University of California, Berkeley, 2103 Etcheverry Hall, USA wtyang@berkeley.edu; tomizuka@berkeley.edu

[2]Hannah Stuart is with the Department of Mechanical Engineering, University of California, Berkeley, 2112 Etcheverry Hall, USA hstuart@berkeley.edu

2023 IEEE International Conference on Soft Robotics (RoboSoft) | 979-8-3503-3222-3/23/$31.00 ©2023 IEEE | DOI: 10.1109/ROBOSOFT55895.2023.10122083

be determined by a uniaxial tensile test. By contrast, we approximate the structure and treat it as a beam, such that fewer parameters must be characterized. By simplifying the model used, we trade off complexity for accessibility. Alici et al. [20] modelled the relationship between air pressure and the bending angle of pneumatic actuators. We expand upon this idea to also predict generated torques for a pneumatic actuator. Hu et al. [8] implemented the analysis of variance (ANOVA) approach to explore optimal parameters, while we mainly use optimization to find the best design parameters. Wang and Hirai [9] also developed a pneumatic actuator by searching each dimensional parameter separately. However, our approach works more efficiently since we propose the mathematical model-based optimal design for the soft actuator. Overall, we seek to produce useful insights to SPA designers in an accessible and fast modeling method by reducing computational complexity.

The remainder of this paper is organized as follows. Section 2 describes our simplified assumptions and mechanical modeling of the SPA. Section 3 discusses the optimal design and fabrication of the SPA. Section 4 demonstrates the experimental results of the soft actuator, and Section 5 concludes the work.

II. Mechanical Modeling of Soft Actuator

SPAs are composed of numerous discrete chambers, and these geometric patterns make their structures irregular. Thus, there lacks an efficient and useful method to model their structures. Instead of treating it as a black box problem, this research considers the soft pneumatic actuator as a continuous beam. The beam structure is a typical example to study bending problems in textbooks [18]. Standard analytical methods could quickly analyze the approximated structure. We, therefore, can obtain a mathematical equation to predict the torques generated by the given input pressures. Furthermore, the mathematical relationship between input and output is used as an objective function. The optimal dimension parameters of the soft actuator can be searched and obtained concerning the objective function.

The simplified structure of the soft actuator is shown in Fig. 1. Some assumptions are made before we begin the analysis process. Firstly, we assume that the actuator elongates within a certain degree and behaves linearly. Soft materials usually exhibit nonlinearity. However, if the elongation is not substantial, the stress-strain curve of general soft materials still approaches a linear relationship. For example, the stress-strain curve of soft silicone rubbers such as Ecoflex Dragon Skin can be approximated as a linear curve at strains below 100 % [21]. Secondly, the soft actuator is mechanically analyzed when the input pressure reaches a steady-state or a quasi-static state. The pressure distributes uniformly inside every chamber in either a steady-state or a quasi-static state.

The mechanical analysis process can be observed in Fig. 2. Figure 2(a) shows that a chamber (a part of the beam) is segmented from the soft actuator. In Fig. 2, the segmented chamber is open on both sides. Since we assume the pressure distributes averagely inside the chamber, the pressure is

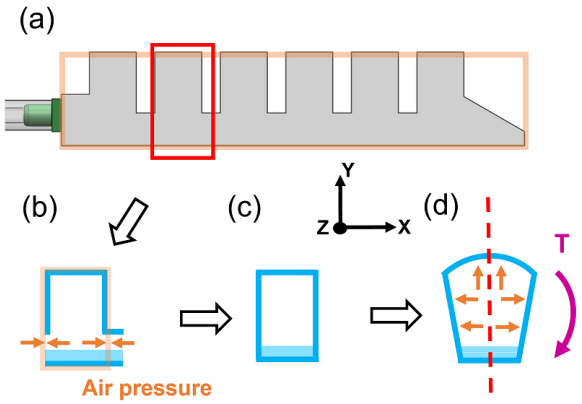

Fig. 2. Mechanical analysis process for the soft pneumatic actuator. (a) A chamber is segmented from the actuator for analysis. (b) The segmented chamber is open on both sides. (c) The open chamber can be considered a closed volume since the air pressure distributes averagely in the chamber and is balanced on the open areas. (d) The air pressure will inflate the chamber to create torques.

balanced in the open areas as shown in Fig. 2(b). We simply consider the segmented chamber as a closed room like Fig. 2(c). Then, as the chamber is pressurized, the air would deform and expand the closed chamber as the Fig. 2(d) and makes the structure generate torque. Since the discrete chambers are approximated as a continuous beam, the mechanical behavior under pressure is continuous in the structure. Thus, we analyze this problem by Eq. (1) and (2)[18]. Equation (1) represents the force balance inside the chamber in x direction in Fig. 2, and Eq. (2) computes the torques generated by the input pressure inside the structure:

$$\sum F_x = \int p(y)dA \tag{1}$$

$$T = \sum T_z = \int y \times p(y)dA \tag{2}$$

where F_x is the force inside the beam in the x direction, $p(y)$ is the pressure function inside the beam and changes along the y direction, T is the torque generated by the actuator, T_z is the torque generated by pressure distribution function $p(y)$, and dA is the small area where the pressure $p(y)$ is located. Note that $p(y)$ is a constant based on the assumption we made.

Before implementing Eq. (1) and (2) to analyze the structure, we need to know the location of the neutral surface where the force and deformation inside the beam are zero under bending [18]. The neutral surface serves as the origin of the generated torques [18]. Unfortunately, the structure of the soft pneumatic actuator has a highly complicated geometric shape. The position of the neutral surface is nonapparent and will vary as the dimensional parameters change in the design stage. We address this issue through a specialized construction of the actuator to enforce a known neutral surface. We embed a sheet of Velostat, a

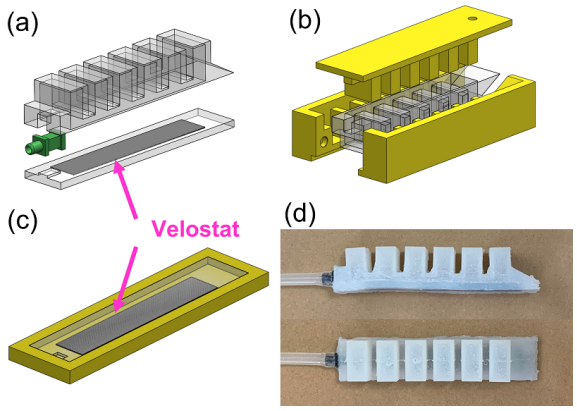

Fig. 3. (a) The exploded view of the soft actuator. Both (b) and (c) show how the upper and lower components are manufactured by two different molds. The appearance of the soft actuator is shown in (d).

compliant but less extensible material, inside the soft actuator as in Fig. 3(a) and (c). The location of the Velostat is the red line in the actuator's cross-section area as shown in Fig. 4(a). By doing so, we assume the neutral surface to be aligned to the black dashed line shown in Fig. 4(a) even if other dimensional parameters change during the design stage. The distance between the Velostat and the neutral surface is around 0.5 mm to account for slight stretching of this material.

With a known neutral surface, we analyze the segmented chamber's free body diagram by slicing it into half as in Fig. 4(b). By using Eq. (1), we solve for the relationship between input pressure and the pressure generated in the wall of the actuator. The free-body diagram of the segmented chamber is shown in Fig. 4(c). The P_w is then described as

$$P_w = \frac{(a-t)(w-2t)}{bw+wt+2at-2t^2}P \tag{3}$$

where a is the distance between the neutral surface and the top of the actuator, b is the distance between the neutral surface and the bottom of the actuator, w is the width of the actuator, and t is the wall thickness as shown in Fig. 4(d). Eq. (2) and Eq. (3) then produce a relationship between P and generated torque T. Therefore, the $T(P)$ can be computed as

$$T(P) = T_P + T_{P_w} \tag{4}$$

where T_P is the torque contributed by P, and T_{P_w} is the torque created by P_w as shown in Fig. 4(b). Since P_w can be replaced by Eq. (3), T_P and T_{P_w} are described by using Eq. (2):

$$T_P = \int y \times P dA_c \tag{5}$$

$$T_{P_w} = \int y \times \frac{(a-t)(w-2t)}{bw+wt+2at-2t^2} P dA_w \tag{6}$$

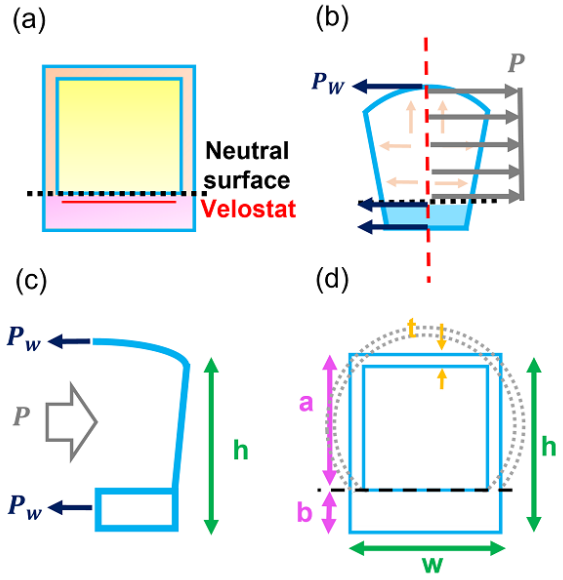

Fig. 4. (a) The cross-section of the chamber is displayed. The black dashed line represents the neutral surface, and the red line is the embedded Velostat. (b) The segmented chamber is cut into half to get the free body diagram. (c) The free-body diagram and the pressures act on it can be observed. (d) The dimension parameters of the cross-section are defined. The dashed gray lines illustrate the expansion of the chamber wall when pressurized.

where dA_c is the arbitrary small area in the cross-section of a chamber (yellow area) in Fig. 4(a), dA_w is the small area in the cross-section of the wall of the actuator (light orange and pink areas in Fig. 4(a)) and y is the location where the pressure acts. The material above the neutral surface is assumed to be in tension, producing positive internal pressures.

In Sec. III, we use the model for $T(P)$ to optimize and select a, b, w and t parameters. We note that the cross-section area of chambers will change significantly with high pressure as the gray dashed line in Fig. 4(d), and this is a known limitation of the proposed method. Therefore, we assume its variation is not significant under limited pressure (< 0.1 MPa). As shown in Sec. IV, we find this idealized assumption to be valid under 0.1 MPa in experiments.

III. Optimal Design Analysis

A. Optimal Design Formulation

We aim to search for the optimal dimension parameters in this subsection. With the derived model in Sec. II, we transform the design problem into a model-based optimization problem [22]. We treat the mathematical model $T(P)$(Eq. (4)) as the objective function subjected to dimension constraints (i.e., a, b, w, and t). The a and b represent the height of the cross-section of the chamber, w means the width, and t is the wall thickness of the soft actuator. The schematic of the dimension parameters in the cross-section of the actuator is displayed in Fig. 4(d). The optimization is defined as:

$$\begin{aligned} &\max_{a,b,w,t} \; T(P) \\ &\text{s.t. } P = constant \\ &\quad a_1 \le a \le a_2 \\ &\quad b_1 \le b \le b_2 \\ &\quad h_1 \le a + b \le h_2 \\ &\quad w_1 \le w \le w_2 \\ &\quad t_1 \le t \le t_2 \end{aligned} \tag{7}$$

where P is a constant value and the constraint parameters a, b, w and t are determined by referencing human fingers' dimensions [9], [23].

The optimization problem is solved by using the optimization toolbox in MATLAB® with the solver `fmincon` with searching step size is 4×10^{-12}. The solution (local minimum) that satisfies the constraints is found when the objective function is non-decreasing. That is, the variation of the objective function is less than the optimality constraint 10^{-6} in all possible searching directions. The optimal design parameters of a, b, w, and t are shown in Table I.

TABLE I

THE PARAMETER SETS VERIFIED BY THE FEA

	a [mm]	b [mm]	w [mm]	t [mm]
Optimal parameters	3.0	17.0	20.0	1.5
Variance 1	3.0	17.0	20.0	2.0
Variance 2	3.0	17.0	20.0	1.75
Variance 3	3.0	17.0	15.0	1.5
Variance 4	3.0	17.0	17.5	1.5
Variance 5	2.0	18.0	20.0	1.5
Variance 6	4.0	16.0	20.0	1.5

The SPA is designed to contain six chambers whose geometric shape is a rectangle. The gap between the chambers and the chamber length is set as 4 mm and 10 mm, respectively. That makes the length of the actuator to be 94 mm, which is approximately the size of a human finger [9], [23]. Next, the model is produced in CAD to run FEA analysis, here using SOLIDWORKS software.

The pneumatic actuator is fixed at the end like a cantilever beam. The tip of the actuator is placed on top of a sensor (steel) and set as the contact condition between them ($\mu = 1$). Hence, the FEA simulation estimates contact force produced by actuation. We assume compliant material to be an isotropic linear elastic according to our assumption in Sec. II. The elastic modulus and Poisson's ratio of the material, Ecoflex® Dragon skin 20, are set as 0.34 MPa and 0.49 [21], [24]. Figure 5 demonstrate the FEA results and the force distribution at the tip, respectively. The mesh sizes are set as 1 mm. On average, the FEA results match true experimental measurements within 90 % (86∼93 %) accuracy. When FEA estimated the force, the torques are obtained by multiplying force with the length of the soft actuator:

$$T_m = F \times L_a \tag{8}$$

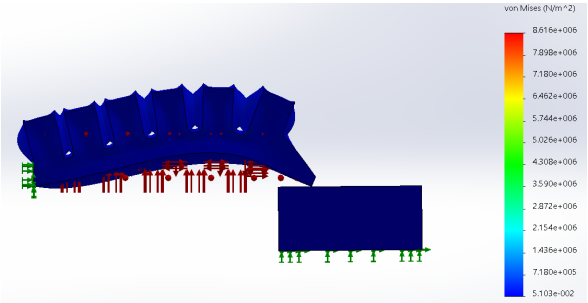

Fig. 5. The FEA of the soft actuator in SOLIDWORKS. The soft actuator is fixed at its end, and the tip contacts a sensor.

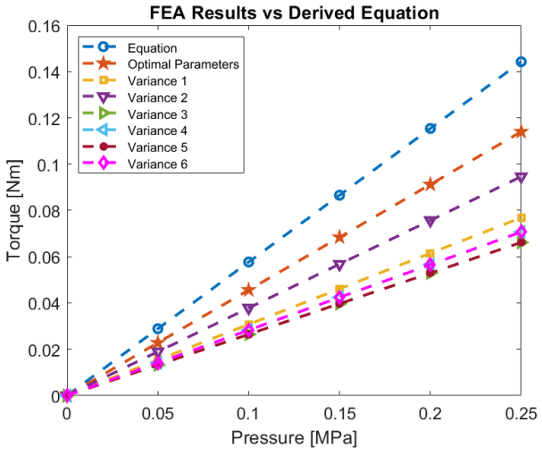

Fig. 6. The FEA results of the pneumatic actuator with the optimal design parameters. In addition, several parameter sets (changing a, b, w and t) are tested in FEA, all showing reduced performance as compared with the optimized parameters.

where T_m is the estimated torque, F is the force, and L_a is the length of the soft actuator.

The FEA results concerning different input pressures are displayed in Fig. 6, in comparison with our simplified model. The prediction of torques by the derived equation as the Eq. (4) (line with circle markers) is higher than the FEA results (line with star markers), however they differ by around 18%. To test sensitivity of the optimally searched solution, we vary the geometric parameters of the soft actuator in FEA analysis to test for better solutions. Six different "variance" alternatives are shown in Fig. 6. The actuators with varied design parameters could not perform as well as those with optimal parameters.

IV. Experimental Evaluation

A. Fabrication of Soft Actuator

The structure of the proposed soft actuator is shown in Fig. 3(a). The actuator body is primarily made of liquid rubber, Ecoflex® Dragon Skin 20. The upper and bottom components in Fig. 3(a) are fabricated by using two different molds as in Fig. 3(b) and (c), inspired by [25]. They are then bonded together by the silicone adhesive, Sil-poxy®. The nozzle at the end is connected to the rubber tube so that the air compressor can input air into the chambers. The

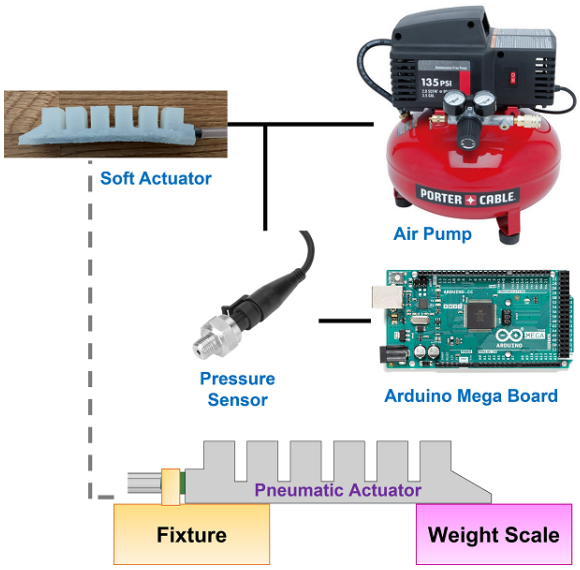

Fig. 7. The schematic of the experimental setup.

bottom component has a piece of Velostat embedded inside to control the position of the neutral surface, inspired by the [19]. The thickness of the thin layer of silicone between the Velostat (red line) and the desired neutral surface (black dashed line) in Fig. 4(a) is controlled to a thickness of 0.5 mm during fabrication. The soft pneumatic actuator is shown in Fig. 3(d). The dimensions of the pneumatic actuator are 20 mm high, 20 mm wide, and 94 mm long.

B. Experimental Setup

The experimental setup is demonstrated in Fig. 7. The soft actuator is actuated by the air compressor (Porter-Cable, Jackson, TN), and the compressor has 4 gallons tank and can generate up to 135 psi (0.9308 MPa). The compressor also has a built-in air pressure regulator. A pressure sensor (Walfront, Lewes, DE) with a sensing range of 0 to 80 psi is implemented to monitor the air pressure and is synchronized with Arduino MEGA 2560 (SparkFun Electronics, Niwot, CO). The microcontroller is based on the Microchip ATmega 2560. The microcontroller is also synchronized with a computer to log sensing data.

C. Test of Torque

The soft pneumatic actuator is designed to optimize the output torque. The fabricated soft actuator is fixed at the end of its structure as in the lower part of Fig. 7. The tip of the soft actuator is contacted on a digital weight scale (Etekcity, Anaheim, CA) with a resolution of 0.01 g and a range of 5 kg. As the air pressure is pumped into the actuator, the actuator inflates and exerts a force on the weight scale. The torque is computed by using Eq. (8). The results in Fig. 8(a) show that the optimized fabricated design ("Design 1") matches closely with modeled results ("Formula"). The maximum torque of the optimal design is 0.144 Nm at the pressure of 0.25 MPa, with other state of the art soft fingers provide 0.085 Nm at the same pressure [3].

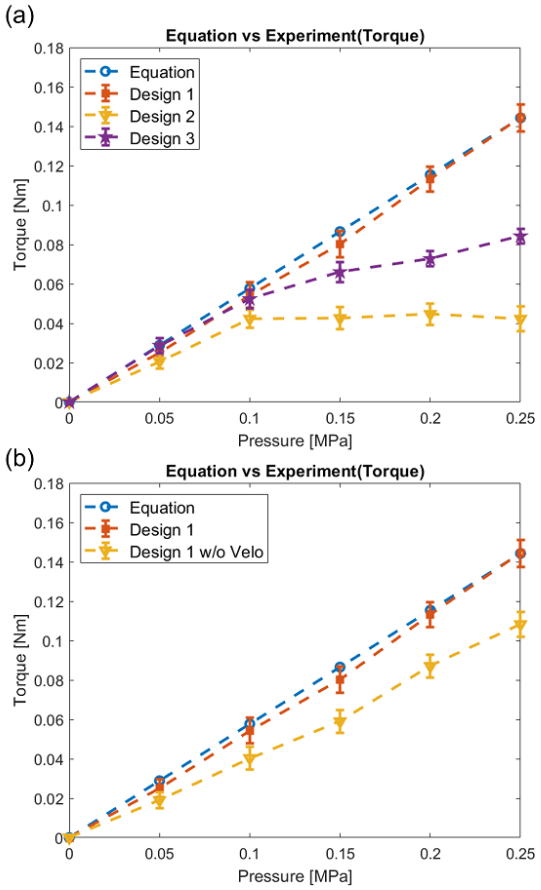

Fig. 8. (a) The experimental validation of optimal designed soft actuator (design 1). A softer material is used in Design 2 and other parameters are the same. Compared to Design 1, Design 3 has a larger length of chamber room. (b) The experimental results of Design 1 without the Velostat. Its performance deviates from the predictions of the derived formula.

Once again, we test alternative designs as a preliminary check for suboptimality ("Design 2" and "Design 3"). Design 2 has a lower Young's modulus of 0.26 MPa (Ecoflex® Dragon skin FX-Pro) as compared with Design 1. Because it is softer, it buckles under higher loads and torque plateaus at 0.046 Nm. The chamber length L of Design 3 is 12 mm larger than that of Designs 1, so L_a is also longer. Its performance drops significantly as the pressure increases, with torque plateauing at 0.090 Nm. All designs perform similarly up to 0.1 MPa of pressure, indicating that the optimization is most useful for higher load applications.

Because we embed a piece of Velostat to manage the position of the neutral surface during fabrication, we make another Design 1 without the Velostat inside and test its performance as shown in Fig. 8(b). Performance deviates more from the estimations of the derived mathematical equation. We suspect that the error arises from a change in the neutral surface of the finger without Velostat, in addition to changes in surface bulging.

D. Test of Bending Angle

The bending angle is another index used to gauge the performance of a soft actuator [8], [9], as soft actuator output

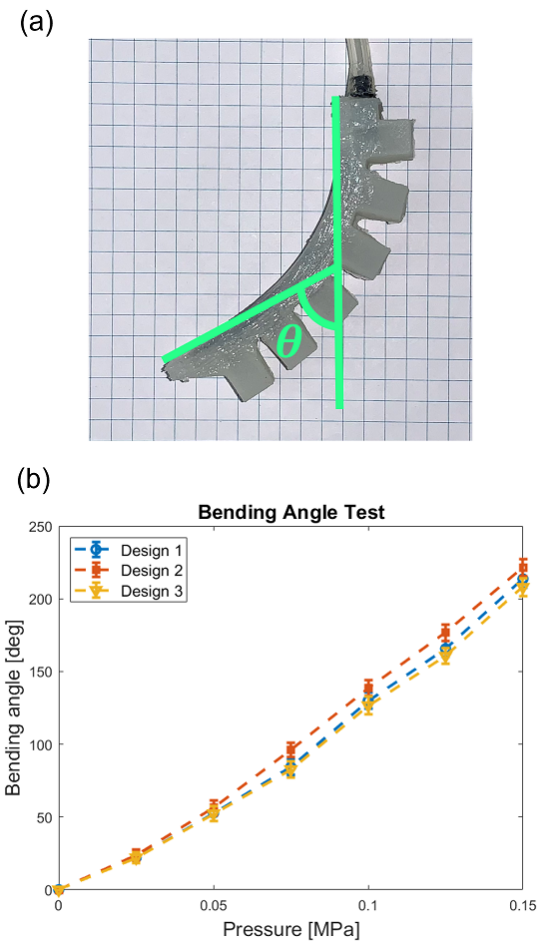

Fig. 9. The bending angle measurement method is disclosed in (a), and the bending angle test results of Designs 1, 2, and 3 are demonstrated in (b).

torque and bending angle are often discussed in tandem. The bendability of the soft actuator is believed to influence the output torque; if the actuator has a large bending angle with fixed input pressure, it is possible to generate more torques [8], [9]. Thus, we also test the bending angle of our design, even though our actuator is optimally designed based on output torque. We define the bending angle as shown in Fig. 9(a) and record it by marking the positions of the tip and end of the actuator on grid paper. By doing so, we can measure the soft actuator's bending angle. In Fig. 9(b), the bending angle test shows that Design 2, with softer material, has the best bending ability. The maximum bending angle of Design 2 is around 221 degrees, while Design 1 and 3 are 214 and 208 degrees, respectively. The bending angle performance of all three designs outperforms recent work [3], which achieved approximately 120 degrees.

V. Discussion

Based on the results in Fig. 8(a) and Fig. 9(b), the linear model assumption appears valid when pressures are less than 0.1 MPa. Although the actuator begins to exhibit nonlinearity with higher pressures, the derived equation Eq. (4) still helps determine a feasible set of parameters. As shown in Sec. IV-C and IV-D, we find a design which outperform both torque and bending angle as compared to an alternative SPA within the same parameter space of interest. In particular, the presented method provides a computationally efficient method to discover soft actuator designs as compared to machine learning and FEA methods. While the assumptions that enable the optimization – a known neutral surface, moderate actuation pressures, no large material deformations outside the linear range – limit the utility across all soft actuator applications, we believe that this rapid modeling method can assist designers interested in this chamber topology to get started quickly and find feasible, useful designs.

An important assumption is the known neutral axis, and we find that the removal of the Velostat layer reduces model accuracy. But the Velostat plays a potential secondary role. In future work, a flex sensor can replace the passive Velostat inside the actuator to measure bending angle. Like in [26], this may be useful if this actuator is utilized to make soft grippers. Various bend sensors are made of thin and largely-inextensible sheeting material.

The equation derived through mechanical derivation does not include the Young's modulus and so it cannot predict the effects of nonideal material properties. As seen with the soft Design 2, this method is less accurate when materials start to experience more buckling and bulging as pressure increases. To test whether the optimal geometry still holds across different softer actuators, we simulated the performance of varying Designs in FEA, all with softer material (Dragon skin FX-Pro). The results are similar to that in Fig. 6, where the optimized parameters continue to outperform selected alternatives as an initial assessment. In addition, the proposed model can be scalable under the assumption of linearity. The optimization algorithm will search the local optima if the constraint space is changed (larger or smaller). Other soft actuator geometries that have more complex chamber shapes, for example, may need to modify the model. Overall this method of testing for real optimality, with a sparse subset of alternatives, is not exhaustive; future work will seek to further test the validity of assumptions.

Ultimately, this method will likely need to be paired with finite element methods to understand performance during higher actuation pressures or with more complex contact conditions. Manufacturing imperfections may influence performance of the model. In order to test this effect, another two prototypes of Design 1 were fabricated. Bending angle varied by approximately $\pm$ 5 degrees and torque varied by $\pm$ 0.025 Nm across all three Design 1 prototypes. Regardless, the present results provide compelling evidence to motivate the use of simple physical models, that can out-perform certain data-driven methods, to guide early soft actuator selection in particular applications.

VI. Conclusions

This work presents a modeling and control strategy for soft pneumatic actuators. Since we simplify the actuator to be a cantilever beam, mechanical analysis can be performed

to model a relationship between pressure and torque. Then, the developed mathematical model serves as the objective function to search for optimal design parameters. The optimal parameters obtained determine the dimension of the soft actuator, which is tested in both FEA and experimentation. The derived optimal design is compared against two other fabricated soft pneumatic actuators, showing that this proposed method can accurately predict and inform improved performance. Moreover, the resulting optimized soft actuator can generate torque up to 0.144 Nm and 214 deg, performing better than a recently developed pneumatic actuator through data-driven design. It is the goal that this mechanically-informed method provides a helpful and efficient tool for rapid design.

REFERENCES

[1] F. Iida and C. Laschi, "Soft robotics: Challenges and perspectives," *Procedia Computer Science*, vol. 7, no. 1, pp. 99–102, 2011.

[2] W.-T. Yang and M. Tomizuka, "Design a multifunctional soft tactile sensor enhanced by machine learning approaches," *ASME Journal of Dynamic Systems, Measurement, and Control*, vol. 144, no. 8, p. 081006, 2022.

[3] K. G. Demir, Z. Zhang, J. Yang, and G. X. Gu, "Computational and experimental design exploration of 3d-printed soft pneumatic actuators," *Advanced Intelligent Systems*, vol. 2, p. 7, 2020.

[4] E. Navas, R. Fernández, D. Sepúlveda, M. Armada, and P. Gonzalez-de Santos, "Soft grippers for automatic crop harvesting: A review," *Sensors*, vol. 21, no. 8, p. 2689, 2021.

[5] S. Zaidi, M. Maselli, C. Laschi, and M. Cianchetti, "Actuation technologies for soft robot grippers and manipulators: A review," *Current Robotics Reports*, pp. 1–15, 2021.

[6] J. Hughes, U. Culha, F. Giardina, F. Guenther, A. Rosendo, and F. Iida, "Soft manipulators and grippers: a review," *Frontiers in Robotics and AI*, vol. 3, p. 69, 2016.

[7] Y. Elsayed, A. Vincensi, C. Lekakou, T. Geng, C. Saaj, T. Ranzani, M. Cianchetti, and A. Menciassi, "Finite element analysis and design optimization of a pneumatically actuating silicone module for robotic surgery applications," *Soft Robotics*, vol. 1, no. 4, pp. 255–262, 2014.

[8] W. Hu, R. Mutlu, W. Li, and G. Alici, "A structural optimisation method for a soft pneumatic actuator," *Robotics*, vol. 7, no. 2, p. 24, 2018.

[9] Z. Wang and S. Hirai, "Chamber dimension optimization of a bellow-type soft actuator for food material handling," in *IEEE International Conference on Soft Robotics (RoboSoft)*, pp. 382–387, IEEE, 2018.

[10] H. Zhang, M. Y. Wang, F. Chen, Y. Wang, A. S. Kumar, and J. Y. Fuh, "Design and development of a soft gripper with topology optimization," in *IEEE/RSJ International Conference on Intelligent Robots and Systems (IROS)*, pp. 6239–6244, IEEE, 2017.

[11] A. Milojević, S. Linß, Ćojbašić, and H. Handroos, "A novel simple, adaptive, and versatile soft-robotic compliant two-finger gripper with an inherently gentle touch," *Journal of Mechanisms and Robotics*, vol. 13, no. 1, p. 011015, 2021.

[12] W. Xiao, D. Hu, W. Chen, G. Yang, and X. Han, "A new type of soft pneumatic torsional actuator with helical chambers for flexible machines," *Journal of Mechanisms and Robotics*, vol. 13, no. 1, p. 011003, 2021.

[13] M. Honarpardaz, "A methodology for design and simulation of soft grippers," *Simulation*, vol. 97, no. 11, pp. 779–791, 2021.

[14] S. Kim, C. Laschi, and B. Trimmer, "Soft robotics: a bioinspired evolution in robotics," *Trends in biotechnology*, vol. 31, no. 5, pp. 287–294, 2013.

[15] D. Rus and M. T. Tolley, "Design, fabrication and control of soft robots," *Nature*, vol. 521, no. 7553, pp. 467–475, 2015.

[16] Z. Xie, A. G. Domel, N. An, C. Green, Z. Gong, T. Wang, E. M. Knubben, J. C. Weaver, K. Bertoldi, and L. Wen, "Octopus arm-inspired tapered soft actuators with suckers for improved grasping," *Soft robotics*, vol. 7, no. 5, pp. 639–648, 2020.

[17] B. Mazzolai, A. ondini, F. Tramacere, G. Riccomi, A. Sadeghi, G. Giordano, E. Del Dottore, M. Scaccia, M. Zampato, and S. Carminati, "Octopus-inspired soft arm with suction cups for enhanced grasping tasks in confined environments," *Advanced Intelligent Systems*, vol. 1, no. 6, p. 1900041, 2019.

[18] R. C. Hibbeler, *Mechanics of materials 8th*. Pearson, New York, 2017.

[19] P. Polygerinos, S. Lyne, Z. Wang, L. F. Nicolini, B. Mosadegh, G. M. Whitesides, and C. J. Walsh, "Towards a soft pneumatic glove for hand rehabilitation," in *IEEE/RSJ International Conference on Intelligent Robots and Systems*, pp. 1512–1517, IEEE, 2013.

[20] G. Alici, T. Canty, R. Mutlu, W. Hu, and V. Sencadas, "Modeling and experimental evaluation of bending behavior of soft pneumatic actuators made of discrete actuation chambers," *Soft robotics*, vol. 5, no. 1, pp. 24–35, 2018.

[21] M. S. Xavier, A. J. Fleming, and Y. K. Yong, "Finite element modeling of soft fluidic actuators: Overview and recent developments," *Advanced Intelligent Systems*, vol. 3, no. 2, p. 2000187, 2021.

[22] D. Trivedi, D. Dienno, and C. D. Rahn, "Optimal, model-based design of soft robotic manipulators," *Journal of Mechanical Design*, vol. 130, no. 9, p. 091402, 2008.

[23] J. Wang, Y. Fei, and W. Pang, "Design, modeling, and testing of a soft pneumatic glove with segmented pneunets bending actuators," *IEEE/ASME Transactions on Mechatronics*, vol. 24, no. 3, pp. 990–1001, 2019.

[24] "Ecoflex Dragon Skin 20." `https://www.smooth-on.com/products/dragon-skin-20/`. Accessed: 2022-06-07.

[25] Z. Wang, K. Or, and S. Hirai, "A dual-mode soft gripper for food packaging," *Robotics and Autonomous Systems*, vol. 125, p. 103427, 2020.

[26] G. Gerboni, A. Diodato, G. Ciuti, and A. Cianchetti, Matteo Menciassi, "Feedback control of soft robot actuators via commercial flex bend sensors," *IEEE/ASME Transactions on Mechatronics*, vol. 22, no. 4, pp. 1881–1888, 2017.